

# Decentralized and Coordinated V-f Control for Islanded Microgrids Considering DER Inadequacy and Demand Control

Buxin She, *Student Member, IEEE*, Fangxing (Fran) Li, *Fellow, IEEE*,  
 Hantao Cui, *Senior Member, IEEE*, Jinning Wang, *Student Member, IEEE*,  
 Orogene Oboreh-Snapps, *Student Member, IEEE*, Rui Bo, *Senior Member, IEEE*

**Abstract**— This paper proposed a decentralized and coordinated voltage and frequency (V-f) control framework for islanded microgrids, with full consideration of the limited capacity of distributed energy resources (DERs) and V-f dependent load. First, we provide a comprehensive discussion of the DER inadequacy concept and the challenges it poses. Then, a decentralized and coordinated control framework is proposed to regulate the output of inverter-based generations and reallocate limited DER capacity for V-f regulation. The control framework is composed of a power regulator and a V-f regulator, which generate the supplementary signals for the primary controller. The power regulator regulates the output of grid-forming inverters according to the real-time capacity constraints of DERs, while the V-f regulator improves the V-f deviation by leveraging the load sensitivity to V-f. Next, the static feasibility and dynamic stability of the proposed method are rigorously proven through mathematical formulation and eigenvalue analysis. Finally, a MATLAB-Simulink simulation demonstrates the functionalities of the control framework. A few goals are fulfilled within the decentralized and coordinated framework, such as making the best use of limited DERs' capacity, enhancing the DC side stability of inverter-based generations, improving power-sharing results, and reducing involuntary load shedding.

**Index Terms**—Islanded microgrid, droop control, coordinated V-f control, DER inadequacy, load power control

## I. INTRODUCTION

A typical microgrid is composed of multiple distributed energy resources (DERs), energy storage systems, and local loads, which can operate in either grid-connected mode or islanded mode. Compared with a conventional bulk power system, microgrids have the characteristics of more DERs, smaller system size [1]-[2], higher uncertainty [3], lower system inertia [4], and stronger voltage and frequency (V-f) coupling [5]-[6]. All of these features create challenges for load-generation balance and V-f regulation in microgrids, especially in islanded microgrids that are not supported by the main grid.

B. She, J. Wang and F. Li are with the Dept. of EECS, The University of Tennessee, Knoxville, TN, USA.

H. Cui is with the School of ECE, Oklahoma State Univ., Stillwater, OK, USA.  
 O. Oboreh-Snapps and R. Bo are with Missouri Univ. of Science and Technology, Rolla, MO, USA.

A hierarchical control framework, which consists of the primary controller, secondary controller, and tertiary controller, has been widely used in islanded microgrids [7]. The primary controller has the lowest bandwidth and is responsible for automatic load sharing. Due to its fast response and important power-sharing functionality, the primary control dominantly determines the V-f deviation and stability of microgrids [8]. Inductive microgrids usually employ the  $P$ - $f$  and  $Q$ - $V$  droop curves in primary control, while resistive microgrids use the reverse  $P$ - $V$  and  $Q$ - $f$  droop curves [9]. In this way, V-f are maintained after normal disturbances like load changes.

An islanded microgrid has many inverter-based generations. As a result of the high penetration of renewable energy, a major cause of grid instability and large V-f deviation pertains to the inadequacy of DERs. DER inadequacy indicates that the capacity of inverter-based generations is sufficient to supply a microgrid's total load. The impacts of limited DER capacity can be seen at both the inverter level and the grid level. For a single inverter, the DC side voltage maintained by the buck-boost converter tends to ripple first and then droop across the linked capacitor when DERs cannot supply enough power [10]. For the whole microgrid, insufficient active and reactive power (P-Q) may result in over frequency and voltage dip [11]. The negative impacts of insufficient DERs necessitate more efficient use of existing generation capacity, which makes the power regulation of inverter-based generations critical in islanded microgrids. The output of grid-following inverters can be controlled easily by changing the  $P_{ref}$  and  $Q_{ref}$ . Grid-forming inverters, on the other hand, make it hard to control power accurately and quickly. Grid-forming inverters are controlled as voltage sources, and their output is mostly determined by the performance of the grid.

Some research has been focused on limiting the output of grid-forming inverters. [12]-[13] designed a current limiter and put it between the current and voltage regulator. The threshold of the current limiter is usually set at 2 p.u. to 3 p.u. because it is designed to prevent high currents in abnormal conditions, e.g., the high currents in low voltage ride through after grounded faults [14]. Apart from the current limiter, [10] and [15] added a virtual impedance to the voltage control loop to limit the terminal voltage of the inverter when its output current is too large. However, the current limiter and virtual impedance

are not suitable for power control of grid-forming inverters because they are mainly designed for protecting the hardware device and cannot accurately control the output of inverters in normal conditions. Moreover, the saturation caused by the current limiter and virtual impedance may result in the instability of the microgrids [16]. In fact, the output of grid-forming inverters in islanded microgrids is determined by the load-sharing results. Their output can be regulated by changing the power-sharing parameters, such as nominal  $P_{ref}$ - $Q_{ref}$  and droop gains. The droop gains are tuned proportionally to DER capacities, allowing each DER to take on new loads according to its capacity [17]. Considering that a DER's capacity may fluctuate from time to time due to its intermittent nature, [18]-[25] developed some adaptive droop strategies, but each with different control targets. [18]-[19] aimed at better reactive power-sharing. [20] focused on better transient performance. [21] presented a method for suppressing circulating current between inverters. [22] addressed inverter-based load control. Although the adaptive control algorithms improve the load sharing results, they are no longer effective if the overall DER capacity is insufficient. This is caused by the saturation of current regulation loop. Thus, a new inverter power regulator considering DER inadequacy has yet to be developed. Further, since P-Q generation shares the same apparent capacity, it is critical to enable the coordination between P-Q generation while regulating the output of inverters [23].

Based on the above discussions, this paper developed a decentralized and coordinated V-f control framework to address DER inadequacy in islanded microgrids. With the proposed control methods, each grid-forming inverter can output any power according to real-time capacity constraints without communicating with adjacent inverters. In addition, demand control [24]-[25] is incorporated into this control framework to reduce load-generation mismatch when DER capacity is insufficient. Demand control leverages load sensitivity to V-f and minimizes involuntary load shedding. Mathematical analysis and simulation results show that demand control collaborates well with inverter output regulator within the decentralized and coordinated framework. The contributions of this paper are as follows.

- We summarize the challenges posed by DER inadequacy in islanded microgrids and address them with full consideration of DER capacity constraints, demand control, and the coordination between P-Q and V-f control.
- We propose a decentralized and coordinated V-f control framework. The control framework can regulate the output of each grid-forming inverter accurately and quickly. It also improves V-f deviation and reduces involuntary load shedding without depending on knowledge and measurements from adjacent nodes.
- We mathematically prove the static feasibility and dynamic stability of the control framework.
- We demonstrate the proposed method using MATLAB-

Simulink in a multi-inverter islanded microgrid.

The rest of this paper is organized as follows. Section II discusses the concept and challenges of DER inadequacy in islanded microgrids, and then introduces the foundation of power and V-f regulation. The decentralized and coordinated V-f control framework is proposed in Section III, followed by theoretical proofs of static feasibility and dynamic stability in Section IV. Section V demonstrates the control method with a modified Banshee microgrid [26]. Conclusions are drawn in Section VI.

## II. DER INADEQUACY IN ISLANDED MICROGRIDS

This section presents the challenges related to DER inadequacy in islanded microgrids and introduces the foundation of the control framework to address these challenges.

### A. Configuration of islanded microgrids

#### 1) Grid-forming inverter

A droop-controlled grid-forming inverter is a basic unit of islanded microgrids. Fig. 1 shows the diagram of a grid-forming inverter supplying static V-f dependent load. The grid-forming inverter is controlled as a voltage source, and the control framework consists of a current regulator, a current limiter, a voltage regulator, and a primary regulator. As a negative feedback controller, the purpose of the primary regulator below is meant to emulate the droop characteristics of conventional synchronous generators and automatically share the load among parallel inverters.

$$\begin{cases} w_{ref} = w_0 - k_{df}(P_m - P_0) \\ V_{ref} = V_0 - k_{dv}(Q_m - Q_0) \end{cases} \quad (1)$$

Where  $P_0$  and  $Q_0$  are initial power setting points;  $P_m$  and  $Q_m$  are measured output;  $k_{df}$  and  $k_{dv}$  are frequency and voltage droop gains, respectively.

#### 2) V-f dependent load

As shown in (2), V-f dependent ZIP loads are modeled in this paper [27].

$$\begin{cases} P_l = P_0(p_1V_l^2 + p_2V_l + p_3)[1 + K_{pf}(f - f_0)] \\ Q_l = Q_0(q_1V_l^2 + q_2V_l + q_3)[1 + K_{qf}(f - f_0)] \end{cases} \quad (2)$$

Where  $V_l$  is the load side voltage;  $p_1+p_2+p_3=1$  and  $q_1+q_2+q_3=1$ ;  $K_{pf}$  is the sensitivity of  $P_l$  to  $f$ ;  $K_{qf}$  is the sensitivity of  $Q_l$  to  $f$ .

The coefficients in (2) represent the compositions of ZIP loads. They change with the time of day and week, seasons, and weather [28], but can be assumed as constant in the timescale of primary control. Because microgrids are usually small in scale, the change in inverter terminal voltage is quickly reflected at the load side, which in turn changes the system demand that depends on the load sensitivity to V-f [8]. As a result, demand control can easily participate in V-f regulation in islanded microgrids.

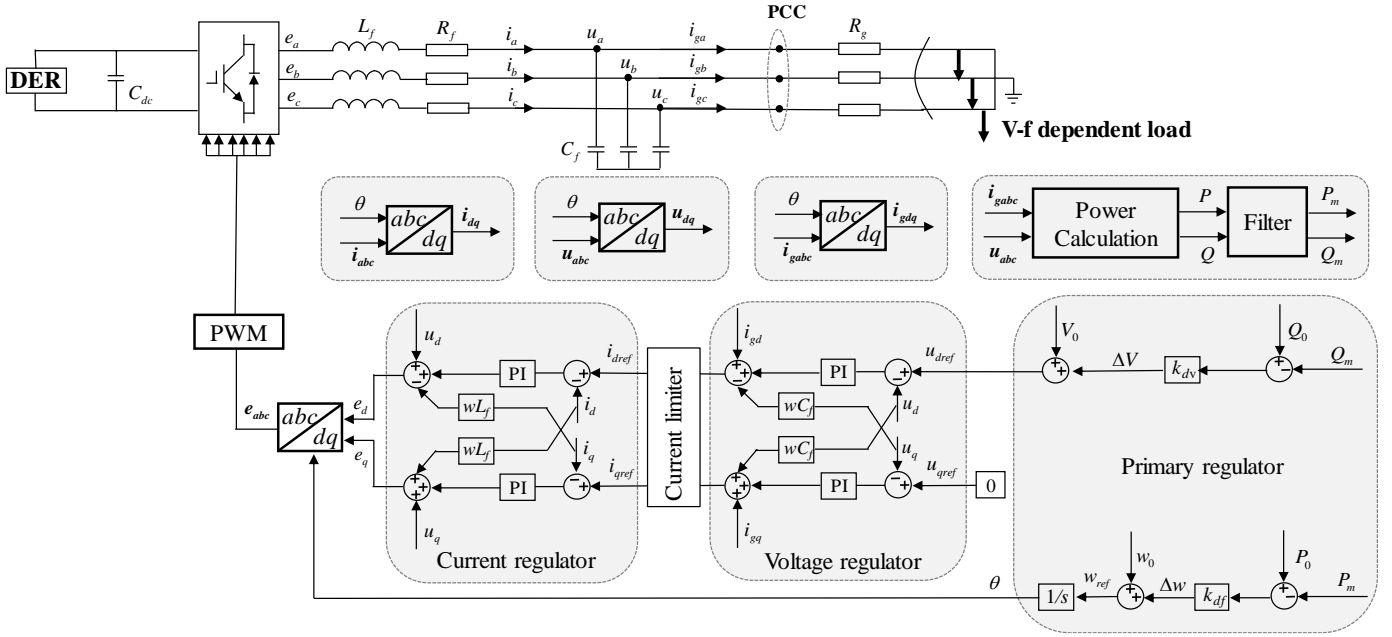


Fig. 1 Diagram of a droop-controlled grid-forming inverter supplying V-f dependent load

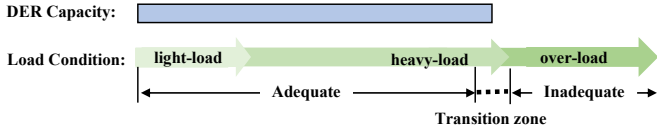


Fig. 2 DER inadequacy under various load level

### B. DER inadequacy and its challenges

An islanded microgrid is a self-sufficient system. DERs pose great challenges to grid operation due to their intrinsic features of uncertainty and intermittency.

#### 1) Load condition and DER inadequacy

Fig. 2 shows a diagram of DER inadequacy under different load levels. With the DER capacity as the baseline, there are generally three load conditions, i.e., light-load, heavy-load, and over-load. 1) In the light-load condition, the total load is much smaller than the DER capacity. Thus, grid V-f may not significantly deviate from the nominal value after normal load change. 2) In the heavy-load condition, the total load is close to, but slightly under, the DER capacity. The output of some grid-forming inverters may exactly equal the capacity of the DC side source. 3) In the over-load condition, the total load is larger than the DER capacity, such that the power balance cannot be guaranteed unless conducting load shedding.

In Fig. 2, if the total load is significantly lower than the generation capacity, the DER is adequate; if the total load is much larger than the generation capacity, the DER is inadequate. The load-generation balance in the critical transition area between the adequate and inadequate zones merits more attention. In this paper, we investigate this critical transition area for its potential to improve stability and reduce large V-f deviation.

#### 2) Challenges

There are three main challenges in islanding microgrids when it comes to DER inadequacy, including improper load sharing, DC side instability, and large V-f deviation.

The first challenge is related to load sharing. In the conventional droop control, the load sharing results are determined by the initial setting point  $[P_0, Q_0]$  and droop gains  $[k_{dp}, k_{dv}]$ . The load change at an equilibrium point is shared proportionally with the droop gains and among the inverters, which are tuned based on the DER capacity. However, due to the intermittency of DERs, their capacities may fluctuate from time to time. The grid-forming inverter has a stability issue if load sharing cannot adapt to the real-time DER capacity [29]. The challenge is more critical in the transition zone shown in Fig. 2 because most grid-forming inverters work in critical states with little reserved capacity.

The second challenge stems from improper load sharing among DERs and is related to DC side voltage. When the shared loads exceed the capacity of the DC side DERs, there is insufficient energy to support the capacitor voltage, which may result in a voltage dip first and then distort Pulse-width modulation (PWM) and power generation. Furthermore, the inverter-based generation will trip and compound the DER inadequacy. Fig. 3(a) shows an unexpected DC voltage dip and generation loss when the shared loads exceed the DER capacity at 5s.

The third challenge relates to large V-f deviation. The first two challenges often impact a single or several inverters, while the third challenge, which is about allocating limited generation capacity to the V-f regulation loop, impacts the whole grid. Fig. 3(b) shows the bounded generation constraint. Following the constraint, V-f regulation results are quite different when implementing different P-Q generation strategies. In general, a large  $k_{df}$  means more active power generation and less

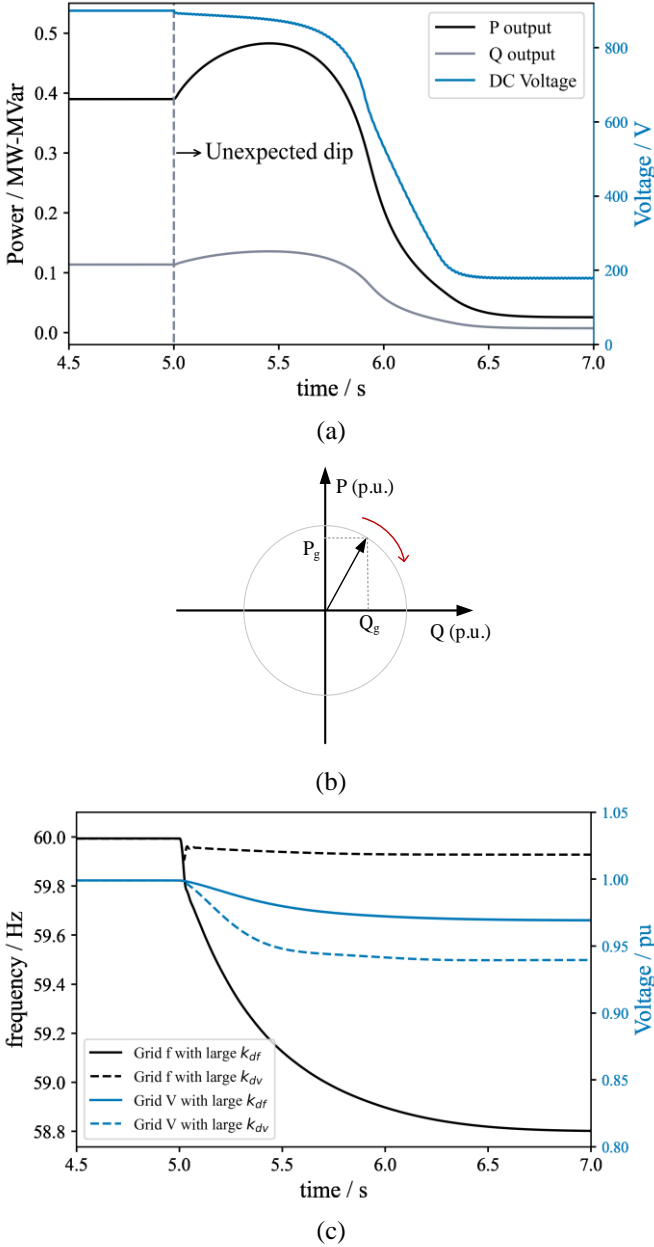


Fig. 3 Challenges related to DER inadequacy (a) DC side voltage dip; (b) Constrained generation capacity among V-f regulation; (c) V-f regulation results with large  $k_{df}$  and large  $k_{dv}$ .

frequency dip, while a large  $k_{dv}$  means more reactive power generation and less voltage dip. Fig. 3(c) shows the V-f regulation results with different droop gains. Usually, the deviation of frequency should be less than 0.01 p.u. and the deviation of voltage should be less than 0.05 p.u.. In Fig. 3(c), the requirements for V-f deviation cannot be met at the same time. V-f deviation can be improved according to the supplementary signals generated by the conventional secondary controller. However, due to saturation caused by the capacity constraints in Fig. 3(b), the inverter may fail to respond to these signals, resulting in an unexpected DC voltage dip.

Considering the challenges discussed above, it is urgent to develop a V-f control framework that can: 1) regulate the output of grid-forming inverters and improve load sharing results

based on real-time DER capacity; 2) adjust P-Q generation under the condition of constrained DER capacity for both acceptable voltage and frequency deviation.

### C. Foundation of the decentralized and coordinated V-f control framework

In Fig. 1, the primary control signals  $w_{ref}$  and  $u_{dref}$  determine the load sharing results and V-f deviation. The foundation of the proposed control method is to design a power regulator and a V-f regulator, which generate the supplementary signals for  $w_{ref}$  and  $u_{dref}$  based on real-time measurements. Specifically, the supplementary signal of the power regulator is generated according to the error between real-time reference capacity  $S_r$  and measured output  $S_m$ , which automatically re-shares the exceeding output among the other inverters. The supplementary signal of the power regulator guarantees the constrained generation shown in Fig. 3(b). Then, like the conventional secondary control, the V-f regulator can further adjust P-Q generation along the boundary and perform load power control through V-f regulation. Finally, the proposed control framework can regulate inverter output and improve V-f deviation at the same time.

As in the conventional droop control, all the supplementary signals are generated depending on local measurements. The proposed control method also enables cooperation between

- *Generation power and load power*: Generation power and load power are regulated simultaneously till reaching a new equilibrium.
- *V regulation and f regulation*: Requirements for V-f deviation are considered at the same time. A tradeoff is made while allocating limited DER capacity for V-f regulation.
- *P generation and Q generation*: Limited DER capacity is allocated to P-loop and Q-loop properly.

As a result, the proposed method is decentralized and coordinated. Section III delves into the control framework.

## III. PROPOSED DECENTRALIZED AND COORDINATED CONTROL FRAMEWORK

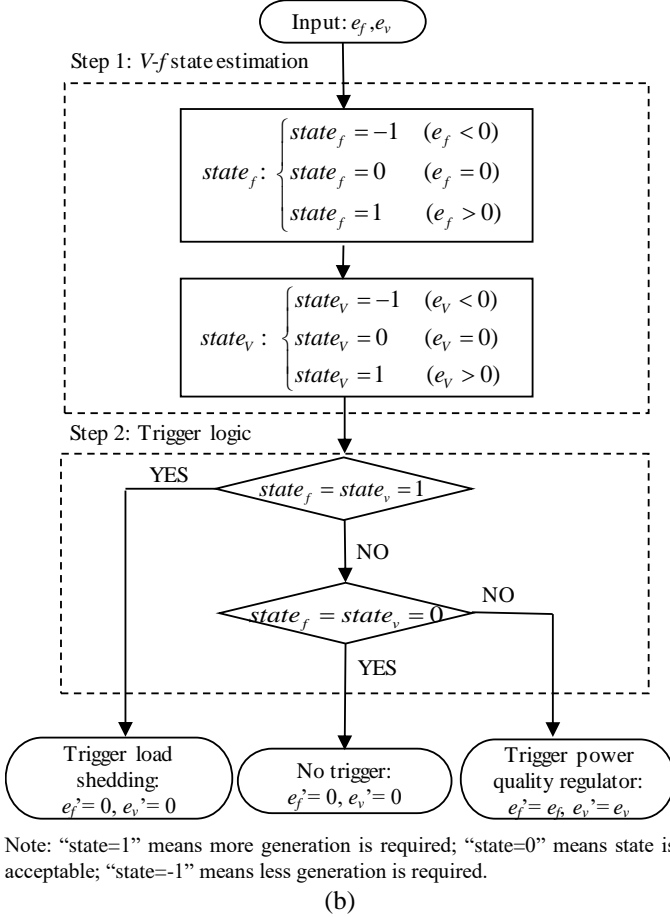
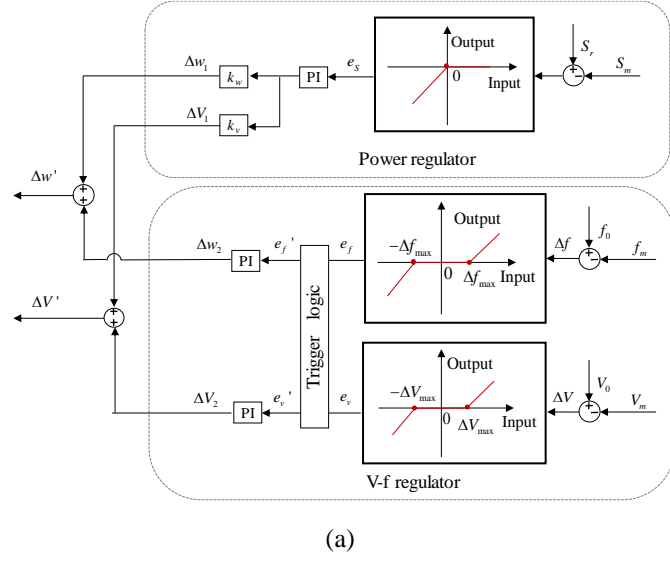
This section introduces the proposed decentralized and coordinated V-f control framework. As shown in Fig. 4(a), the control framework consists of a power regulator and a V-f regulator. They are implemented locally, generating supplementary signals  $\Delta w'$  and  $\Delta V'$  for the primary controller of each grid-forming inverter.

### A. Power regulator

The transfer function of the power regulator is shown in (3)-(4).

$$\begin{bmatrix} \Delta w_1 \\ \Delta V_1 \end{bmatrix} = (k_{ps} + \frac{k_{is}}{s}) e_s \begin{bmatrix} k_w \\ k_v \end{bmatrix} \quad (3)$$

$$e_s = \begin{cases} 0 & S_r > S_m \\ S_m - S_r & S_r \leq S_m \end{cases} \quad (4)$$



Note: “state=1” means more generation is required; “state=0” means state is acceptable; “state=-1” means less generation is required.

Fig. 4 Diagram of decentralized and coordinated control: (a) control framework (b) trigger logic of V-f regulator

The errors between  $S_r$  and  $S_m$  are fed to a proportional-integral (PI) controller, which is then allocated to the frequency and voltage regulation loop according to regulation gains  $k_w$  and  $k_v$ , respectively. Typically, if the inverter outputs more power than  $S_r$ ,  $e_s$  is negative, and the inverter will decrease its output by decreasing the terminal voltage and angle frequency.

### B. V-f regulator

The transfer function of the V-f regulator is shown in (5)-(7).

$$\begin{bmatrix} \Delta w_2 \\ \Delta V_2 \end{bmatrix} = \begin{bmatrix} k_{pf} + \frac{k_{if}}{s} & 0 \\ 0 & k_{pv} + \frac{k_{iv}}{s} \end{bmatrix} \mathbf{Tr} \begin{bmatrix} e_f \\ e_v \end{bmatrix} \quad (5)$$

$$e_f = \begin{cases} \Delta f + \Delta f_{\max} & \Delta f < -\Delta f_{\max} \\ 0 & -\Delta f_{\max} \leq \Delta f \leq \Delta f_{\max} \\ \Delta f - \Delta f_{\max} & \Delta f > \Delta f_{\max} \end{cases} \quad (6)$$

$$e_v = \begin{cases} \Delta V + \Delta V_{\max} & \Delta V < -\Delta V_{\max} \\ 0 & -\Delta V_{\max} \leq \Delta V \leq \Delta V_{\max} \\ \Delta V - \Delta V_{\max} & \Delta V > \Delta V_{\max} \end{cases} \quad (7)$$

Where  $\Delta f = f_0 - f_m$ ,  $\Delta V = V_0 - V_m$ , and  $\mathbf{Tr}$  is the trigger logic. If we assume  $dS/dV > 0$  and  $dS/df > 0$ , then the diagram of the trigger logic is shown in Fig. 4(b), which considers the relationship between V-f regulation and load-generation balance. The trigger logic judges whether the existing DER capacity is adequate or not to meet V-f deviation requirements. For example,  $state_f = state_v = 1$  means V-f droop too much at the same time, and both V-f regulation loops need more generation capacity. This means that the existing DER capacity is not enough to regulate V-f, so load shedding will be needed.

The power regulator has priority over the V-f regulator because it guarantees the capacity constraints that are closely related to DC voltage stability. Hence, a power regulator usually has larger controller gains and larger bandwidth than a V-f regulator.

## IV. STATIC FEASIBILITY AND DYNAMIC STABILITY

This section proves static fixability and dynamic stability of the proposed control framework through algebraic formulation and eigenvalue analysis.

### A. Static feasibility

The proposed control framework has two main functionalities: 1) regulate the output of inverters through load re-sharing; 2) improve V-f deviation by reallocating generation capability along the constrained boundary in Fig. 3(b). The mechanism of load re-sharing is similar to that of the adaptive droop gain method, which has been clearly illustrated in existing literature [21]. Hence, this subsection mainly verifies the second functionality through algebraic formulation.

The V-f regulator is identical to the conventional secondary controller when DER capacity is adequate, which improves V-f deviation by adjusting the output of inverter-based generations. It changes to a constrained secondary controller in the transition zone when the load is close to the total generation. It reallocates the limited generation to V-f regulation loops following the output constraints. Focusing on the system in Fig. 1, the stability feasibility validation considers the V-f dependent load model in (2) and the output constraints in Fig. 3b. Then, the validation has three steps as follows.

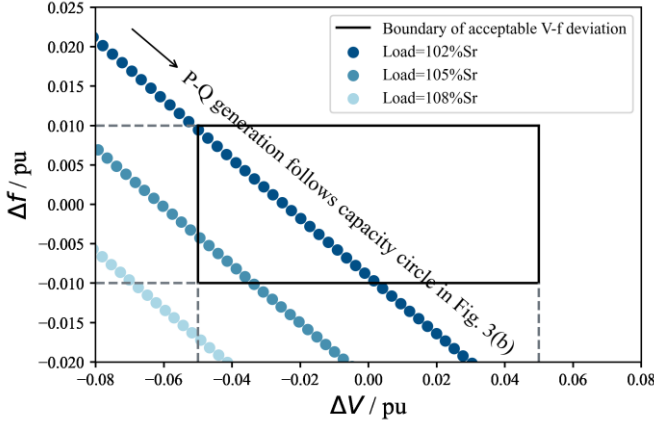


Fig. 5 V-f deviation under bounded generation constraints

$$\begin{cases}
 \text{step 1:} & \begin{cases} P_0' = P_0 + \Delta P \\ Q_0' = Q_0 + \Delta Q \end{cases} \\
 \text{step 2:} & \begin{cases} V\text{-}f: \begin{cases} V' = V + \Delta V \\ f' = f + \Delta f \end{cases} \\
 \text{Load:} & \begin{cases} P_l' = P_0'(p_1 V_l'^2 + p_2 V_l' + p_3)(1 + K_{pf} \Delta f) \\ Q_l' = Q_0'(q_1 V_l'^2 + q_2 V_l' + q_3)(1 + K_{qf} \Delta f) \\ V_l' = V' + V_{loss} \end{cases} \\
 \text{Generation:} & P_g'^2 + Q_g'^2 = S^2 \end{cases} \\
 \text{step 3:} & \begin{cases} P_g' = (1 + r_p \%) P_l' \\ Q_g' = (1 + r_q \%) Q_l' \end{cases} \\
 \text{step 4:} & \text{New equilibrium } P_g', Q_g', P_l', Q_l', \Delta V \text{ and } \Delta f.
 \end{cases} \quad (8)$$

Where  $P_0$  and  $Q_0$  are the initial loads;  $V$  and  $V'$  are the terminal voltage of the inverter before and after the load change;  $V_l$  and  $V_l'$  are the load side voltage before and after the load change;  $V_{loss}$  is the voltage droop on the grid line;  $r_p$  and  $r_q$  represent the rate of power loss on the grid line;  $P_g'$ ,  $Q_g'$  and  $P_l'$ ,  $Q_l'$  are the new generation and load.

Equation (8) predicts the new equilibrium after an intentional load change in the transition zone, where the conventional primary controller becomes invalid. In step 1, an intentional load increases at the current operating point ( $P_0$ ,  $Q_0$ ). The inverter generation that was originally represented by the droop equation is updated to a bounded constraint named ‘‘Generation’’ in step 2, Eq. (8). Then, a new equilibrium is reached, satisfying the generation-load balance in step 3.

We use the algebraic formulation in (8) to predict the V-f deviation of the system shown in Fig. 1 under various load increases. Fig. 5 presents the predicted new equilibriums implementing different generation strategies, where the total load is slightly larger than the bounded generation after the intentional load increase. Based on Fig. 5, we make the following observations:

- For Load=102% $S_r$  and Load=105% $S_r$ , although the total load is larger than the generation capacity, load-generation balance can still be achieved without performing load shedding because there are some new equilibriums inside

the black security rectangle that meet the V-f deviation requirements.

- If the current operating point locates outside the black security rectangle where the V-f regulator may be triggered, the P-Q generation can be adjusted along the bounded generation circle until the operating point comes back to the acceptable region.
- If the total load is too large, e.g. Load=108% $S_r$ , load shedding is required since there is no operating point inside the security rectangle. But the shed load could be less than conventional strategies so as to reduce unnecessary involuntary shedding. For example, 3% to 5% is enough to improve V-f deviation using demand control.

The steady-state formulation verifies the effectiveness of P-Q regulation following the bounded capacity for acceptable V-f deviation, which lays the foundation of the proposed control framework.

### B. Dynamic stability

A small-signal model is built up to verify the dynamic stability of the proposed control framework.

#### 1) Small-signal modeling

The comprehensive dynamic model is composed of some differential equations in  $s$  domain and algebraic equations [30]. We integrate the proposed power regulator and V-f regulator into the conventional droop control controller in Fig. 1. Then, we derive the complete dynamic model in the form of a set of differential-algebraic equations (DAEs) as follows.

$$\begin{cases} \dot{\mathbf{x}} = \mathbf{f}(\mathbf{x}, \mathbf{y}) \\ 0 = \mathbf{g}(\mathbf{x}, \mathbf{y}) \end{cases} \quad (9)$$

where  $\mathbf{x}$  is the state variable and  $\mathbf{x} = [\varphi_{vs}, \varphi_{fs}, \varphi_v, \varphi_f, \varphi_{ud}, \varphi_{uq}, \varphi_{id}, \varphi_{iq}, \varphi_p, u_d, u_q, i_d, i_q, P_m, Q_m, i_{gd}, i_{gq}]$ ;  $\mathbf{y}$  is the algebraic variable and  $\mathbf{y} = [u_{dref}, u_{qref}, i_{dref}, i_{qref}, e_d, e_q, P, Q]$ .

After linearizing the DAEs in (9), we obtain the small-signal model in (10). Then, we calculate the state matrix  $\mathbf{A}$  by eliminating the algebraic variables. Considering that the V-f regulator contains piecewise functions, each linear part may be analyzed according to initial operating points.

$$\begin{bmatrix} \Delta \dot{\mathbf{x}} \\ 0 \end{bmatrix} = \begin{bmatrix} \mathbf{f}_x & \mathbf{f}_y \\ \mathbf{g}_x & \mathbf{g}_y \end{bmatrix} \begin{bmatrix} \Delta \mathbf{x} \\ \Delta \mathbf{y} \end{bmatrix} \quad (10)$$

$$\mathbf{A} = \mathbf{f}_x - \mathbf{f}_y \mathbf{g}_y^{-1} \mathbf{g}_x \quad (11)$$

#### 2) Eigenvalue analysis

We then choose an operating point outside the black security rectangle in Fig. 5 and calculate the eigenvalues of  $\mathbf{A}$ . Fig. 6 shows the relevant eigenvalues when  $[k_w, k_v] = [0.1, 0.22]$ . For the sake of illustration, only the real part larger than -20 is presented. In Fig. 6, the real part of the eigenvalues all lies in the left half-plane except for the origin, which verifies the stability of the control framework.

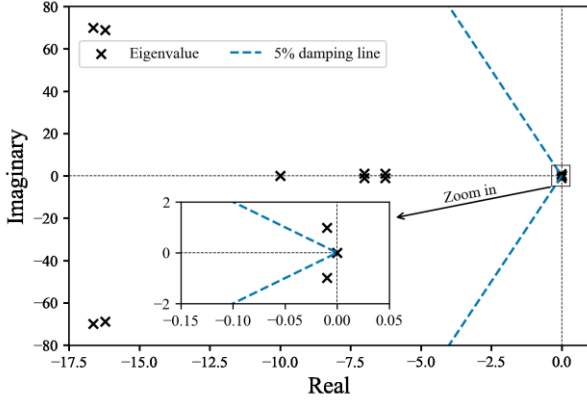


Fig. 6 Relevant eigenvalues of A matrix

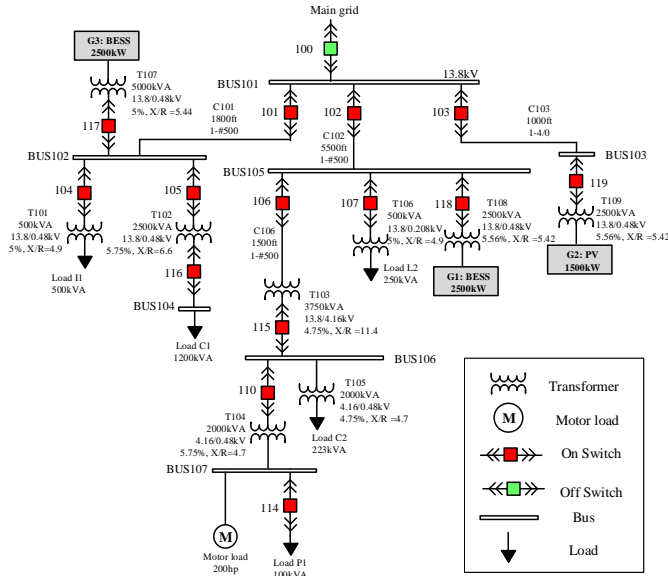


Fig. 7. Single line diagram of the islanding microgrid [26]

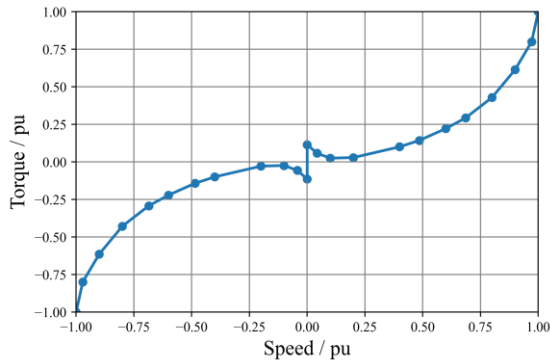


Fig. 8. The torque-speed curve of motor load [26]

TABLE I  
ZIP LOAD PARAMETERS

Load	P composition/ [ $p_1, p_2, p_3$ ]	Q composition/ [ $q_1, q_2, q_3$ ]	V-f sensitivity/ [ $k_{pf}, k_{qf}$ ]
L1	0.1, 0.3, 0.6	0.5, 0.3, 0.2	2, -0.1
L2	0.6, 0.2, 0.2	0.6, 0.2, 0.2	2.5, -2
C1	0.5, 0.3, 0.2	0.2, 0.3, 0.5	3, -0.1
C2	0.4, 0.3, 0.3	0.4, 0.3, 0.3	1, -0.5
P2	0.5, 0.3, 0.2	0.5, 0.3, 0.2	3, -1

## V. CASE STUDY

### A. Case overview

The microgrid shown in Fig. 7 operates in islanded mode with switch 100 off. It is modified from the Banshee distribution system by replacing the diesel generator on BUS 103 with a battery energy storage system (BESS) and connecting a PV and a BESS to BUS 102 and 105, respectively [26]. The three grid-forming inverters are named G1, G2, and G3 in Fig. 7. The microgrid also supplies the static V-f dependent ZIP load and motor load, and their parameters are listed in Tab. 1 and Fig. 8.

All of the simulations below were run in MATLAB® version R2020a, with a PC Intel® Core i7-8665U CPU at 2.10 GHz and 16 GB RAM.

### B. Test results

Two test scenarios are designed to validate the key functionalities of the proposed control framework. Scenario 1 focuses on inverter power regulation, while scenario 2 focuses on the cooperation of the power regulator and V-f regulator, which leverage the limited DER capacity and demand control to improve V-f deviation and reduce involuntary load shedding.

#### 1) Scenario 1: inverter power regulation

Following the timeline, the basic settings of Scenario 1 are three-fold:

- Before 8s, G1-G3 are controlled with the conventional droop method represented in Fig. 1.
- At 8s, the inverter power regulators of G1-G3 are implemented and triggered immediately. Meanwhile, the real-time reference capacities of G1-G3 are set as 1.2MVA, 0.6MVA, and 2.0 MVA, respectively.
- At 12s, load C2 connected to Bus 106 increases by 200kW, 100kVar.

Fig. 9 shows the microgrid performance in Scenario 1, where Fig. 9(a) is the dynamic output of G1-G3, Fig. 9(b) is the static output, and Fig. 9(c) is the dynamic voltage and frequency.

In Fig. 9(a), the output of G1 and G3 follows the left axis, while the output of G2 follows the right axis, based on which we have the following observations:

- According to the initial setting point ( $P_0, Q_0$ ) and droop gains ( $k_{df}, k_{dv}$ ) before 8s, all the load is automatically shared among G1, G2, and G3 as 1.24MVA, 0.67MVA, and 1.24MVA, respectively.
- At 8s, S1 and S2 violate the real-time capacity constraints, and the power regulator starts working. Then, P1, Q1, P2, and Q2 decrease until S1 and S2 are regulated to the reference value.
- Even though there is a sudden load increase at 12s, S1 and S2 still converge to the reference value. Meanwhile, P3, Q3, and S3 increase at 8s and 12s to compensate for the decreased generation and the increased load.

Fig. 9(b) further presents three static operating points at 6s, 10s, and 14s. In Fig. 9(b), the circle and square operating points of G1 and G2 lie exactly on the capacity boundary after triggering the power regulator.

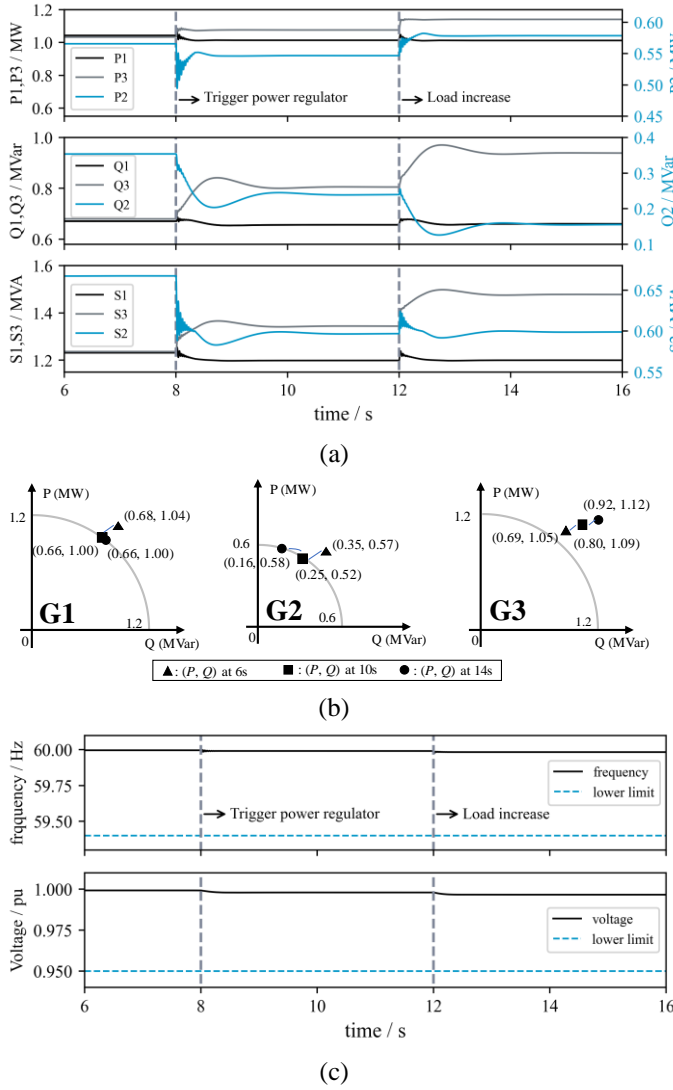


Fig. 9. Microgrid performance in Scenario 1 (a) dynamic inverter output; (b) static inverter output; (c) dynamic frequency and voltage

TABLE II  
CONTROL PARAMETERS OF G3 IN SCENARIO 2

Scenario	Droop gains / $[k_{df}, k_{dv}]$	Power	V-f
		regulator gains / $[k_{ps}, k_{is}, k_r, k_v]$	regulator gains / $[k_{pf}, k_{if}, k_{pv}, k_{iv}]$
2-1	[0.01, 0.05]	[0.50, 10.00, 0.04, 0.50]	[10.00, 20.00, 5.00, 5.00]
2-2	[0.01, 0.07]	[0.50, 10.00, 0.06, 0.20]	[5.00, 0.50, 5.00, 5.00]

In Fig 9(c), the voltage and frequency are measured at the terminal of G3, and they hardly change after the power regulator starts working. This means the power regulator can regulate the output of inverters without disturbing the grid voltage and frequency too much.

## 2) Scenario 2: cooperation of power regulator and V-f regulator

In the transition zone shown in Fig. 2, the conventional primary and secondary controllers become invalid due to the saturation caused by insufficient DER capacity. Then, the steady-state V-f is mainly determined by the V-f regulator gains ( $k_f, k_v$ ). Scenario 2 is further divided into two parts, Scenario 2-

1 and Scenario 2-2, to show the cooperation of the power regulator and V-f regulator under different ( $k_f, k_v$ ). Focusing on G3, Scenario 2-1 has a large  $k_v$  and large voltage dip that crosses the boundary of V-f deviation, while Scenario 2-2 has a large  $k_f$  and an unacceptable frequency dip. The control parameters of G3 are presented in Tab. II.

Following the timeline, Scenario 2-1 and Scenario 2-2 have the same settings as follows, and their grid performance is shown in Figs. 10-12.

- Before 8s, G1-G3 are controlled with the conventional droop method represented in Fig. 1.
- At 8s, load C2 increases by 200kW, 100kVar.
- At 12s, the reference capacities of G1-G3 are set as 1.2MVA, 0.6MVA, and 1.2 MVA, respectively. The total load is thus larger than the total generation capacity, and the power regulator starts working.
- At 16s, the V-f regulator starts working.

Fig. 10 and Fig. 11 show the dynamic and static inverter output, respectively. They both validate the functionalities of the power regulator and V-f regulator.

In Fig. 10, as a result of different droop gains, Scenario 2-1 and Scenario 2-2 have distinct load sharing results after load change at 8s. For example, G3 has a larger  $k_{dv}$  in Scenario 2-2, so it outputs less reactive power than that in Scenario 2-1. At 12s, the power regulator starts working. S1, S2, and S3 are regulated to 1.2MVA, 0.6MVA, and 1.2 MVA, respectively, around 12.5s, which are exactly equal to the reference capacities. The reduced generation is compensated by the load response to V-f regulation (load power decreases as V-f decrease). S1-S3 remain unchanged after triggering the V-f regulator at 16s, indicating that the power regulator and the V-f regulator work well together.

Fig. 11 shows the static operating points at 6s, 10s, 14s, and 18s. After the power regulator is turned on, the circle and square operations of G1-G3 all fall on the constrained boundary.

Fig. 12 shows the dynamic frequency and voltage measured at the terminal of G3. Both frequency and voltage have an obvious dip at 12s because the total load is larger than the generation capacity. To achieve load-generation balance again, the load power decreases after the voltage and frequency dip. Scenario 2-1 and Scenario 2-2 have different V-f regulation results due to distinct power regulator gains. Scenario 2-1 has a large  $k_v$  and thus a larger voltage dip, while Scenario 2-2 has a large  $k_f$  and thus a larger frequency dip. From 12s to 16s, the voltage in Scenario 2-1 and the frequency in Scenario 2-2 violate the requirements of V-f deviation. The violations are mitigated after the trigger of the V-f regulator at 16s.

In general, Scenarios 2-1 and 2-2 verify the proposed decentralized and coordinated control framework. The framework enables output control of grid-forming inverters and V-f improvement under the condition of constrained DER capacity.



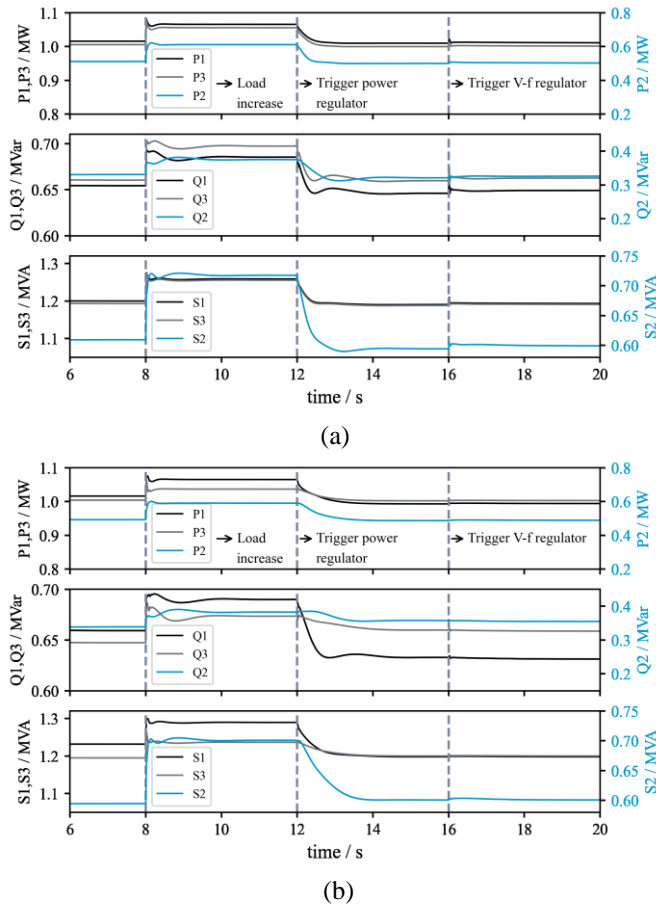


Fig. 10. Dynamic inverter output: (a) Scenario 2-1; (b) Scenario 2-2

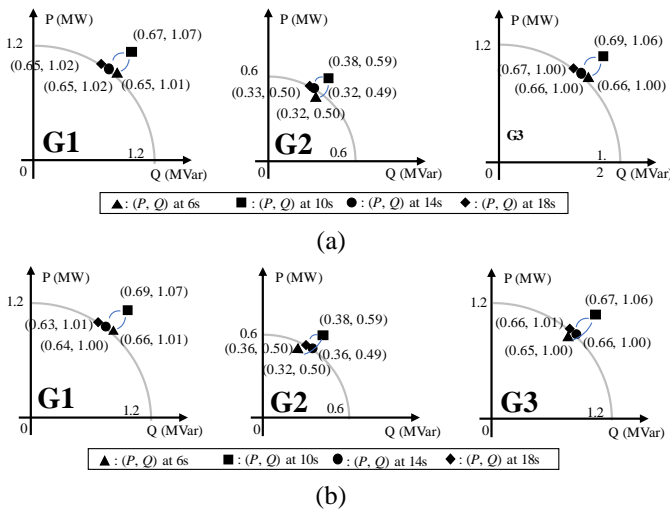


Fig. 11. Static inverter output: (a) Scenario 2-1; (b) Scenario 2-2

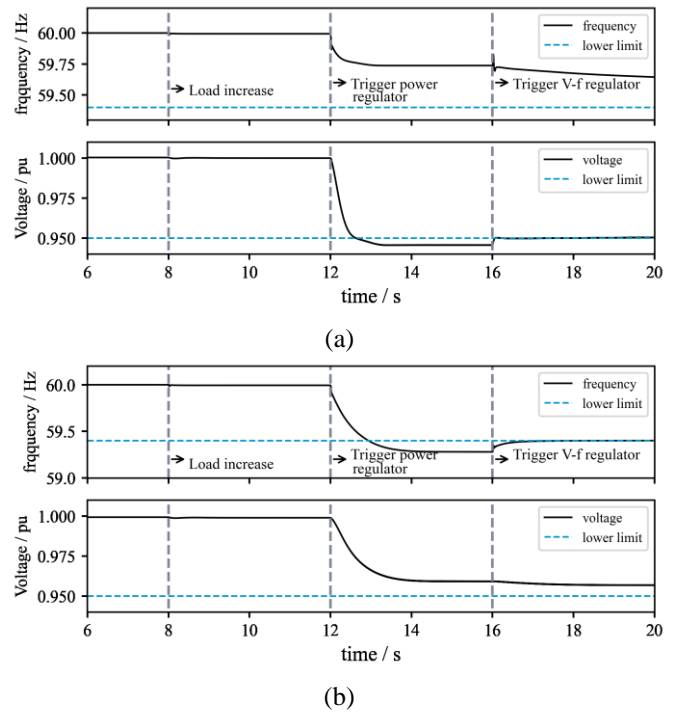


Fig. 12. Dynamic frequency and voltage (a) Scenario 2-1; (b) Scenario 2-2

## VI. CONCLUSION

This paper proposes a decentralized and coordinated V-f control framework to address the challenges brought by DER inadequacy in islanded microgrids. The control framework is composed of a power regulator and a V-f regulator. The power regulator can regulate the output of grid-forming inverters without violating real-time reference capacities, while the V-f regulator improves the V-f deviation by leveraging the load response to voltage and frequency. The control framework is developed based on conventional droop control and is thus purely decentralized and not dependent on costly communication interfaces. In addition, it guarantees DC voltage stability and reduces involuntary load shedding. Within the proposed control framework, three-level coordination is achieved simultaneously when DERs are inadequate, including 1). Generation power and load power, 2). V regulation and f regulation, and 3). P generation and Q generation.

This paper focuses mostly on V-f control at the primary level. In the future, detailed energy management strategies that generate real-time reference capacity will be investigated.

## REFERENCES

- [1] X. Jiang, J. Xiao, B. She, and G. Zu, "Locating and sizing of partition flexible interconnection converter station in large urban power grids," *IET Generation, Transmission & Distribution*, vol. 13, no. 21, pp. 4830–4841, Sep. 2019, doi: 10.1049/iet-gtd.2018.6871.
- [2] X. Kou *et al.*, "Model-Based and Data-Driven HVAC Control Strategies for Residential Demand Response," *IEEE Open Access Journal of Power and Energy*, vol. 8, pp. 186–197, 2021, doi: 10.1109/OAJPE.2021.3075426.

- [3] M. N. Ahmed, M. Hojabri, A. M. Humada, H. B. Daniyal, and H. Fahad, "An Overview on Microgrid Control Strategies," vol. 4, no. 5, p. 6.
- [4] Z. Qu, J. C.-H. Peng, H. Yang, and D. Srinivasan, "Modeling and Analysis of Inner Controls Effects on Damping and Synchronizing Torque Components in VSG-Controlled Converter," *IEEE Transactions on Energy Conversion*, vol. 36, no. 1, pp. 488–499, Mar. 2021, doi: 10.1109/TEC.2020.3010049.
- [5] P. Sun, J. Yao, Y. Zhao, X. Fang, and J. Cao, "Stability Assessment and Damping Optimization Control of Multiple Grid-connected Virtual Synchronous Generators," *IEEE Transactions on Energy Conversion*, pp. 1–1, 2021, doi: 10.1109/TEC.2021.3104348.
- [6] S. Sivaranjani, E. Agarwal, V. Gupta, P. Antsaklis, and L. Xie, "Distributed Mixed Voltage Angle and Frequency Droop Control of Microgrid Interconnections With Loss of Distribution-PMU Measurements," *IEEE Open Access Journal of Power and Energy*, vol. 8, pp. 45–56, 2021, doi: 10.1109/OAJPE.2020.3047639.
- [7] P. Singh, P. Paliwal, and A. Arya, "A Review on Challenges and Techniques for Secondary Control of Microgrid," *IOP Conf. Ser.: Mater. Sci. Eng.*, vol. 561, p. 012075, Nov. 2019, doi: 10.1088/1757-899X/561/1/012075.
- [8] M. Farrokhhabadi *et al.*, "Microgrid Stability Definitions, Analysis, and Examples," *IEEE Trans. Power Syst.*, vol. 35, no. 1, pp. 13–29, Jan. 2020, doi: 10.1109/TPWRS.2019.2925703.
- [9] C. Sun, G. Joos, and F. Bouffard, "Adaptive Coordination for Power and SoC Limiting Control of Energy Storage in an Islanded AC Microgrid With Impact Load," *IEEE Transactions on Power Delivery*, vol. 35, no. 2, pp. 580–591, Apr. 2020, doi: 10.1109/TPWRD.2019.2916034.
- [10] R.-J. Wai, Q.-Q. Zhang, and Y. Wang, "A Novel Voltage Stabilization and Power Sharing Control Method Based on Virtual Complex Impedance for an Off-Grid Microgrid," *IEEE Transactions on Power Electronics*, vol. 34, no. 2, pp. 1863–1880, Feb. 2019, doi: 10.1109/TPEL.2018.2831673.
- [11] W. Feng, Q. Shi, H. Cui, and F. Li, "Optimal power allocation strategy for black start in VSC-MTDC systems considering dynamic impacts," *Electric Power Systems Research*, vol. 193, p. 107023, 2021, doi: 10.1016/j.epsr.2021.107023.
- [12] A. Gkountaras, S. Dieckerhoff, and T. Sezi, "Evaluation of current limiting methods for grid forming inverters in medium voltage microgrids," in *2015 IEEE Energy Conversion Congress and Exposition (ECCE)*, Montreal, QC, Canada, Sep. 2015, pp. 1223–1230. doi: 10.1109/ECCE.2015.7309831.
- [13] Xunwei Yu and Zhenhua Jiang, "Dynamic current limiting control of voltage source inverters," in *2009 IEEE International Electric Machines and Drives Conference*, Miami, FL, USA, May 2009, pp. 1664–1668. doi: 10.1109/IEMDC.2009.5075427.
- [14] N. Bottrell and T. C. Green, "Comparison of Current-Limiting Strategies During Fault Ride-Through of Inverters to Prevent Latch-Up and Wind-Up," *IEEE Trans. Power Electron.*, vol. 29, no. 7, pp. 3786–3797, Jul. 2014, doi: 10.1109/TPEL.2013.2279162.
- [15] J. Chen, D. Yue, C. Dou, L. Chen, S. Weng, and Y. Li, "A Virtual Complex Impedance Based  $\$P-\dot{V}\$$  Droop Method for Parallel-Connected Inverters in Low-Voltage AC Microgrids," *IEEE Transactions on Industrial Informatics*, vol. 17, no. 3, pp. 1763–1773, Mar. 2021, doi: 10.1109/TII.2020.2997054.
- [16] W. Du *et al.*, "A Comparative Study of Two Widely Used Grid-Forming Droop Controls on Microgrid Small-Signal Stability," *IEEE J. Emerg. Sel. Topics Power Electron.*, vol. 8, no. 2, pp. 963–975, Jun. 2020, doi: 10.1109/JESTPE.2019.2942491.
- [17] M. M. Bijaich, W. W. Weaver, and R. D. Robinett, "Energy Storage Requirements for Inverter-Based Microgrids Under Droop Control in d-q Coordinates," *IEEE Transactions on Energy Conversion*, vol. 35, no. 2, pp. 611–620, Jun. 2020, doi: 10.1109/TEC.2019.2959189.
- [18] D. K. Dheer, Y. Gupta, and S. Doolla, "A Self-Adjusting Droop Control Strategy to Improve Reactive Power Sharing in Islanded Microgrid," *IEEE Transactions on Sustainable Energy*, vol. 11, no. 3, pp. 1624–1635, Jul. 2020, doi: 10.1109/TSTE.2019.2933144.
- [19] Y. Gupta, K. Chatterjee, and S. Doolla, "A Simple Control Scheme for Improving Reactive Power Sharing in Islanded Microgrid," *IEEE Transactions on Power Systems*, vol. 35, no. 4, pp. 3158–3169, Jul. 2020, doi: 10.1109/TPWRS.2020.2970476.
- [20] S. Prakash, V. Nougain, and S. Mishra, "Adaptive Droop-Based Control for Active Power Sharing in Autonomous Microgrid for Improved Transient Performance," *IEEE Journal of Emerging and Selected Topics in Power Electronics*, vol. 9, no. 3, pp. 3010–3018, Jun. 2021, doi: 10.1109/JESTPE.2020.2988712.
- [21] N. Ghanbari and S. Bhattacharya, "Adaptive Droop Control Method for Suppressing Circulating Currents in DC Microgrids," *IEEE Open Access Journal of Power and Energy*, vol. 7, pp. 100–110, 2020, doi: 10.1109/OAJPE.2020.2974940.
- [22] S. Chaturvedi, D. Fulwani, and J. M. Guerrero, "Adaptive-SMC Based Output Impedance Shaping in DC Microgrids Affected by Inverter Loads," *IEEE Transactions on Sustainable Energy*, vol. 11, no. 4, pp. 2940–2949, 2020, doi: 10.1109/TSTE.2020.2982414.
- [23] A. Vasilakis, I. Zafeiratou, D. T. Lagos, and N. D. Hatziargyriou, "The Evolution of Research in Microgrids Control," *IEEE Open Access Journal of Power and Energy*, vol. 7, pp. 331–343, 2020, doi: 10.1109/OAJPE.2020.3030348.
- [24] E. S. N. Raju P. and T. Jain, "A Two-Level Hierarchical Controller to Enhance Stability and Dynamic Performance of Islanded Inverter-Based Microgrids With Static and Dynamic Loads," *IEEE Transactions on Industrial Informatics*, vol. 15, no. 5, pp. 2786–2797, 2019, doi: 10.1109/TII.2018.2869983.
- [25] M. Langwasser, G. De Carne, M. Liserre, and M. Biskoping, "Voltage-Based Load Control for Frequency Support Provision by HVDC Systems," in *IECON 2018 - 44th Annual Conference of the IEEE Industrial Electronics Society*, Oct. 2018, pp. 311–316. doi: 10.1109/IECON.2018.8592709.
- [26] R. Salcedo *et al.*, "Banshee distribution network benchmark and prototyping platform for hardware-in-the-loop integration of microgrid and device controllers," *J. eng.*, vol. 2019, no. 8, pp. 5365–5373, Aug. 2019, doi: 10.1049/joe.2018.5174.
- [27] M. Cui, M. Khodayar, C. Chen, X. Wang, Y. Zhang, and M. E. Khodayar, "Deep Learning-Based Time-Varying Parameter Identification for System-Wide Load Modeling," *IEEE Trans. Smart Grid*, vol. 10, no. 6, pp. 6102–6114, Nov. 2019, doi: 10.1109/TSG.2019.2896493.
- [28] C. Wang, Z. Wang, J. Wang, and D. Zhao, "Robust Time-Varying Parameter Identification for Composite Load Modeling," *IEEE Transactions on Smart Grid*, vol. 10, no. 1, pp. 967–979, 2019, doi: 10.1109/TSG.2017.2756898.
- [29] B. Pawar, E. I. Batzelis, S. Chakrabarti, and B. C. Pal, "Grid-Forming Control for Solar PV Systems With Power Reserves," *IEEE Transactions on Sustainable Energy*, vol. 12, no. 4, pp. 1947–1959, 2021, doi: 10.1109/TSTE.2021.3074066.
- [30] F. Milano, *Power System Modelling and Scripting*, vol. 0. Berlin, Heidelberg: Springer Berlin Heidelberg, 2010. doi: 10.1007/978-3-642-13669-6.